

A Comparative Study of Three Speckle Reducing Methods for Intima-Media Thickness Ultrasound Images

Mehravar Rafati¹; Masoud Arabfard²; Mehrdad Rafati Rahimzadeh³; Hasan Voshtani^{4,*}; Hassan Moladoust⁴

¹Department of Medical Physic and Radiology, Faculty of Paramedical Sciences, Kashan University of Medical Sciences, Kashan, IR Iran

²Department of Basic Sciences, Kish International Campus, University of Tehran, Kish Island, IR Iran

³Department of Nursing, Babol University of Medical Sciences, Babol, IR Iran

⁴Department of Cardiology, Heshmat Cardiovascular Research Center, Guilan University of Medical Sciences, Rasht, IR Iran

*Corresponding Author: Hasan Voshtani, Department of Cardiology, Heshmat Cardiovascular Research Center, Guilan University of Medical Sciences, Rasht, IR Iran. Tel: +98-1333663070, Fax: +98-1316668718, E-mail: voshtanihasan@yahoo.com

Received: October 30, 2014; **Revised:** November 24, 2014; **Accepted:** December 31, 2014

Background: Ultrasonic evaluation of intima-media thickness (IMT) is an early marker of assessing the development of atherosclerosis and determining cardiovascular risk. To attain the best possible diagnosis, it is essential that medical images be clear, sharp and without noise and artifacts.

Objectives: Comparison of speckle reducing anisotropic diffusion (SRAD), discrete (DTD) and continuum topological derivative (CTD) on B-mode ultrasound images of common carotid and brachial arteries throughout the cardiac cycle.

Patients and Methods: In a cross-sectional design, an examination was performed on forty-two human subjects with a mean age of 44 ± 6 years from April 2013 to June 2013. This study was approved by the ethics committees of Kashan University of Medical Sciences and Beheshti Hospital. An ultrasonic examination of common carotid and brachial arteries of forty-two human subjects was performed. The program was designed in MATLAB software to extract consecutive B-mode images and apply region of interest (ROI) on the IMT of the common carotid and brachial arteries. Then, three different noise reduction filters with the Canny edge detection were used in ROI separately. Finally, the program measured the image quality metrics.

Results: According to values of eleven different image quality metrics (mentioned in the main text), there was a significant difference between CTD, DTD and SRAD filters with the Canny edge detection status in the common carotid and brachial arteries throughout the cardiac cycle (all P values < 0.001). For example, peak signal to noise ratios (PSNR) using CTD, DTD and SRAD filters were 95.43 ± 0.64, 88.86 ± 0.82 and 73.02 ± 0.20 in common carotid and 96.39 ± 1.25, 92.58 ± 0.11 and 88.27 ± 0.63 in brachial arteries, respectively (both P values < 0.001).

Conclusions: By measuring image quality metrics, this study showed that DTD and CTD filters with the Canny edge detection respectively, are better than SRAD filter with the Canny detection for speckle suppression and details preservation in both arteries in the ultrasound images.

Keywords: Carotid Intima-Media Thickness; Brachial Artery; Ultrasonography; Noise

1. Background

Intima-media thickness (IMT) of the carotid artery and its increase is associated with several cardiovascular risk factors and manifest cardiovascular disease (CVD) (1, 2). The walls of the common carotid artery are straight and run parallel to the skin's surface. The walls of the proximal internal carotid artery are usually divergent and curvilinear, and the vessel frequently descends deeper into the neck and is no longer parallel to the skin's surface. Even without such detractors as acoustic shadowing, which can occur when lesions are present, it is to be expected that measurements of the common carotid artery would be usually more precise than those of the internal carotid artery (3). Moreover, the pattern of wall thickening in brachial artery is quite diffuse than carotid artery, which may be a more sensitive index of long systemic exposure to risk

factors (4). Therefore, evaluating mechanical parameters changes of common carotid and brachial arteries attracted researcher's attention. Using ultrasound for this aim is proper, because it is a noninvasive and non-radiation method. Its cost is low and it has capability of forming real time imaging (5). To attain the best possible diagnosis, it is essential that medical images be clear, sharp and without noise and artifacts. By nature, ultrasound image includes a lot of noise contents, especially speckle noise than other imaging modalities (6). Speckle artifact is produced by interference of energy from randomly distributed scattering. It reduces image resolution and contrast and blurs necessary details; thereby, speckle noise reduces diagnostic value of this imaging modality. Therefore, speckle noise reduction is essential whenever ultrasound imag-

ing is used (6, 7). The traditional speckle removal filters, like the Lee filter and Frost filter have greater restrictions in edge preserving and characteristics preserving (8). Yu et al. presented the speckle reducing anisotropic diffusion (SRAD) filter (9) based on a partial differential equation (PDE). The PDE-based speckle removal approach allows the generation of set of filtered images that vary from fine to coarse. This filter is not sensitive to filter window size and shape (9). SRAD not only protects edges, but also enhances edges by eliminating diffusion across edges and allowing diffusion on either side of the edge (8). Besides, the topological derivative is a branch of computational mathematics with the aim of solving problems when the domain under consideration is perturbed by introduction of heterogeneity (10). Discrete topological derivative (DTD) algorithm is an indicator function that finds best pixels to introduce the holes or cracks that would most reduce noise conserving suitable image features in presence of diffusion (11). Continuum topological derivative (CTD) algorithm goes through a gradual transition from one state to a different state, without sudden changes (11). CTD finds scaling parameter for the cost function and percentages of pixel that is re-classified in iteration and DTD calculates fined weighted for both terms in the cost function. Indeed, DTD describes difference between perturbed and original cost functions (12). Thus, it is essential to have noise reduction filters to preserve the features, so that noise reduction causes no blurred or distorted edges.

2. Objectives

The aim of this study was to analyze performance of SRAD, DTD and CTD filters in ultrasound images of common carotid and brachial arteries for optimum removing noise with preservation of edges.

3. Patients and Methods

3.1. Study Protocol

In a cross-sectional design, an examination was performed on forty-two human subjects with a mean age of 44 ± 6 years from April 2013 to June 2013. Traditionally, atherosclerosis disease is considered a typical middle-age disease. CVD, the most frequent and lethal form of atherosclerosis disease, reaches a significant incidence at the age of 40 years in men (13). Our study group consisted of healthy volunteers who came to Beheshti hospital affiliated to Kashan University of Medical Sciences. It is a governmental hospital. Patients' medical history, physical examination, electrocardiography (ECG) and echocardiography were recorded. None of the subjects had history of cardiovascular and/or cerebrovascular disease, hypertension, diabetes mellitus and tobacco abuse (14). All subjects gave informed consent prior to participation in the study. This study was approved by the ethics committees of Kashan University of Medical Sciences and Beheshti Hospital (Iran; Code ethical ap-

proval, 9139; Approval date, 05/08/2012). In our study, before ultrasonography, subjects rested for at least 10 minutes in supine position until their heart rate and blood pressure reached a steady state. Blood pressure and heart rate were recorded with a calibrated oscilloscopic blood manometer (ALP K2, Adult Cuff, ± 1 mmHg, Tokyo, Japan) and a wrist manometer (Microlife, ± 3 mmHg, Germany) on the left brachial and radial arteries with the subject in a supine position respectively. Measurements were performed in a temperature-controlled room according to current guidelines (15). The left common carotid of subjects, 2 - 3 cm proximal to the bifurcation and the left brachial artery (3-5 cm upper than elbow) were examined in the longitudinal direction with a high resolution Sonoline Antrases (Siemens, HenkestraBe, Erlangen, Mittelfranken, Bayern, Germany) ultrasound system equipped with a 5 - 13 MHz linear transducer (16). Dynamic range, depth of focus, maximum display depth, acoustic aperture, number of elements, array length and spatial pulse length were 55 dB, 3.5 cm, 6 cm, 45×9 mm, 192×3 , 39 mm and 55, respectively (17). The audio video interleaves (AVI) format of the consecutive images of the common carotid and brachial arteries with a frame rate of 43 frames per second was captured from hard drive and transferred to a PC (computer) for post processing. The recording contained 90 frames (almost three cardiac cycles), while the left common carotid and brachial arteries were scanned in the longitudinal direction. A program was designed using MATLAB software version 7.01 (Math Software Co., Math Works, USA) to extract consecutive images in the bitmap (BMP) format from the AVI (image size: 547×692 pixel²). Images were normalized so that the average gray scale median of the pixels in blood ranged between 0 and 5, whereas that of the adventitia as 180-190 according to widely accepted specifications (18). Region of interest (ROI) with a size of approximately 53×42 pixel² applied on the IMT of the posterior wall of common carotid and brachial arteries (19). Then, different noise reduction filters (SRAD, DTD and CTD) with the Canny edge detection were performed in ROI separately. Finally, the program measured mean squared error (MSE) (20), peak signal to noise ratio (PSNR) (20), normalized absolute error (NAE) (19, 20), normalized cross-correlation (NCC) (21), structure similarity image measures (SSIM) (22), speckle index (SI) (20), structural content (SC) (23), image quality index (IQI) (20, 21), maximum difference (MD) (23), average difference (AD) (23) and equivalent number of looks (ENL) (18, 24) (Table 1). All measurements of both arteries were performed by a single operator to eliminate inter-observer variability (25).

3.2. Off-Line Analysis

The Canny edge detection algorithm was applied in this study using Matlab software. It uses a multi-stage algorithm to detect various edges in images. For finding edges, this detector searches local maximum of the gradient of the image function ($f(x, y)$).

Table 1. Performance Metrics and Their Mathematical Definitions

| Performance | Mathematical Expression | Purpose |
|--|--|---|
| Mean square error (MSE) | $MSE = \frac{1}{MN} \sum_{i=1}^m \sum_{j=1}^n (x(i, j) - y(i, j))^2$, Where $x(i, j)$ represents the original image and $y(i, j)$ represents the de-noised image and i and j are the pixel position of the $M \times N$ image. MSE is zero when $x(i, j) = y(i, j)$ A higher/lower MSE value corresponds to maximum/minimum difference between the original and de-noised image. | The MSE is the average of the square of the difference between original and de-noised image intensity values divided by the size of the image (20). The MSE is used to find total amount of average difference between two images. |
| Peak signal to noise ratio (PSNR) | $PSNR = 10 \log_{10} \frac{(2^n - 1)^2}{\sqrt{MSE}}$ Where n is the number of bits used in presenting the pixel of the image. For example, grayscale image, n is 8. | It is a ratio between the maximum possible power of the signal and the noise content. Higher PSNR value shows better image quality (20). |
| Normalized Absolute Error (NAE) | $NCC = \frac{\sum_{i=1}^M \sum_{j=1}^N x_{i,j} - y_{i,j} }{\sum_{i=1}^M \sum_{j=1}^N (x(i,j))^2}$, Where $x(i, j)$ represents the original image and $y(i, j)$ represents the de-noised image and i and j are the pixel position of the $M \times N$ image. | It measures the error perdition accuracy of the image. Large value of NAE indicates poor quality (19, 22). |
| Normalized Cross Correlation (NCC) | $x NCC = \frac{\sum_{i=1}^M \sum_{j=1}^N (x(i,j)y(i,j))}{\sum_{i=1}^M \sum_{j=1}^N (x(i,j))^2}$, Where $x(i, j)$ represents the original image and $y(i, j)$ represents the de-noised image and i and j are the pixel position of the $M \times N$ image. Its value is unity for identical images. | The closeness between two digital images can also be quantifies for correlation function. Normalized Cross Correlation measures the similarity between two images. Its value would approach 1 as difference between the two images approaches 0 (21). |
| Speckle Index (SI) | $NCC = \frac{\sum_{i=1}^M \sum_{j=1}^N (x(i,j)y(i,j))}{\sum_{i=1}^M \sum_{j=1}^N (x(i,j))^2}$, Where i and j are the pixel position of the $M \times N$ image. σ, μ are variance and mean, respectively. | It is measure of average contrast of an image. A low SI value for effective de-speckling. Usually the speckle index changes from 1 to a lesser value (20). |
| Structural Content (SC) | $SC = \frac{\sum_{i=1}^M \sum_{j=1}^N x_{i,j}^2}{\sum_{i=1}^M \sum_{j=1}^N (y_{i,j})^2}$, Where $x(i, j)$ represents the original image and $y(i, j)$ represents the de-noised image and i and j are the pixel position of the $M \times N$ image. Its value is unity for identical images. | It measures similarity between the original and de-noised images. Reconstructed image is of good quality if SC value lies near 1, greater values indicate poor quality image (23). |
| Equivalent Numbers of Looks (ENL) | $ENL = (NMV)^2 / (NSD)^2$, $NSD = \frac{1}{MN} \sqrt{(\sum I(x,y) - NMV)^2}$, $x=1, \dots, m$ and $y=1, \dots, n$, Noise Mean Value (NMV) = $(1/(m*n)) \sum I(x,y)$, $x=1, \dots, m$ and $y=1, \dots, n$, Where I is de-noised image, m represents the number of rows and n represents the number of columns in the image. NMV is mean and NSD is standard deviation is measure of the signal to noise ratio. | To estimate the speckle noise level another assessment parameter known as ENL over a uniform region is used. A larger value of ENL shows a better quantitative performance (24, 26). |
| Image Quality Index (IQI) | $IQI = \frac{4\sigma_{xy}\bar{x}\bar{y}}{(\sigma_x^2 + \sigma_y^2) \left(\left(\frac{\bar{x}}{\sigma_x} \right)^2 + \left(\frac{\bar{y}}{\sigma_y} \right)^2 \right)}$, $\bar{x}, \bar{y}, \sigma_x, \sigma_y$ and σ_{xy} are given as $\bar{x} = \frac{1}{N} \sum_{i=1}^N x_i$ and $\bar{y} = \frac{1}{N} \sum_{i=1}^N y_i$, $\sigma_x^2 = \frac{1}{N-1} \sum_{i=1}^N (x_i - \bar{x})^2$ and $\sigma_y^2 = \frac{1}{N-1} \sum_{i=1}^N (y_i - \bar{y})^2$ $\sigma_{xy} = \frac{1}{N-1} \sum_{i=1}^N (x_i - \bar{x})(y_i - \bar{y})$ | It is a combination of three factors such as loss of correlation, mean distortion and variance distortion. The range of image quality index is [-1]. For identical images, the value of images, the value of image quality index is unity (20, 21). |
| Maximum Difference (MD) | $MD = \max x(i,j) - y(i,j) $, Where $x(i, j)$ represents the original image and $y(i, j)$ represents the de-noised image and i and j are the pixel position of the $M \times N$ image. | MD is the maximum of the error signal (difference between the reference signal and test image). Large value of MD means that the image is poor quality (23). |
| Average Difference (AD) | $AD = \frac{1}{MN} \sum_{i=1}^M \sum_{j=1}^N (x(i, j) - y(i, j))$, Where $x(i, j)$ represents the original image and $y(i, j)$ represents the de-noised image i and j are the pixel position of the $M \times N$ image. | AD is simply the average of difference between the reference signal and test image. A lower value of MD means that image is poor quality (23). |
| Structural Similarity Index Metric (SSIM) | $SSIM = \frac{(2\bar{x}\bar{y} + C_1)(2\sigma_{xy} + C_2)}{(\sigma_x^2 + \sigma_y^2 + C_2) \left(\left(\frac{\bar{x}}{\sigma_x} \right)^2 + \left(\frac{\bar{y}}{\sigma_y} \right)^2 + C_1 \right)}$, $\bar{x}, \bar{y}, \sigma_x^2, \sigma_y^2$ and σ_{xy} are given as: $\bar{x} = \frac{1}{N} \sum_{i=1}^N x_i$, $\bar{y} = \frac{1}{N} \sum_{i=1}^N y_i$, $\sigma_x^2 = \frac{1}{N-1} \sum_{i=1}^N (x_i - \bar{x})^2$, and $\sigma_{xy} = \frac{1}{N-1} \sum_{i=1}^N (x_i - \bar{x})(y_i - \bar{y})$ | The SSIM is the best method to evaluate image quality. Two images would have good similarity if SSIM value is 1 and poor if it is lesser than 0.9 (22). |

The gradient is calculated using the derivative of a Gaussian filter. There are two different thresholds to detect strong and weak edges and weak edges are connected to the strong edges in this method. In this study, we assumed here that the speckle pattern in ultrasound images has a white, Gaussian noise model (26-28) and for consecutive images, the Canny edge detection with different common de-speckling methods (SRAD, DTD, and CTD filters) were performed in ROI on the IMT of the posterior wall of common carotid and brachial arteries. Speckle has multiplicative properties in the nature. There are a number of elementary scatters within each resolution cell. Speckle noise with a random granular pattern corrupts the acquired image and delays interpretation of image content (27). A speckle image is commonly modeled as multiplicative noise in ultrasound images (26, 28). The SRAD method (29, 30) is used directly for suppressing speckle noise in ultrasound images with instant coefficient. That is based on PDE including the imaging gradient, Laplacian and image intensity. SRAD equation used in this study is given in Equation 1:

Where t is the diffusion time index, Δt is the time step responsible for the convergence rate of the diffusion process (range: 0.05 to 0.25) and $g(\text{ICOV}(u'))$ is the diffusion function and is given by Equations 2 and 3

$$(1) \text{SRAD}(U') = ut+1 = ut + (\frac{\Delta t}{4}) \text{div}(g(\text{ICOV}(u')) \nabla * xu')$$

$$(2) \quad G(\text{ICOV}(u')) = e - (P)$$

$$(3) \quad P = \frac{((\text{ICOV}(U')q^t)^2 - 1)}{(1+q^t)^2}$$

Where q is the measure of speckle coefficient of variation in a homogenous region of the image. CTD is known as the real line or on the correspond cardinal number. Continuum is anything that goes through a gradual transition from one condition to a different condition without any abrupt changes. A single point is a continuum that contains more than one point (11). It is the same as discrete but designed vector $b = \{\varphi_1, \varphi_2, \dots, \varphi_n\}$. $\varphi_1, \varphi_2, \dots, \varphi_n$ are structures that modeled as a continuum. Topological derivative quantifies the sensitivity of a problem when the domain is perturbed by the introduction of heterogeneity (31, 32). Let the domain Ω under consideration is perturbed by the introduction of small holes (topology changes) in Ω as shown in Figure 1. In this Ω Ω is the domain under perturbation, γ_ϵ is the crack of length centered at the pixel n , $\Psi(\Omega)$ is the cost function assigned before perturbation and $\Psi(\Omega/\gamma_\epsilon)$ is the cost function after perturbation. We considered bounded open set in R^N ($N = 2, 3$) and γ_ϵ as a crack of length centered at point $x \in \Omega$ (11, 12):

Where $f(\epsilon)$ is known positive function going to zero

with, and $D_T(x)$ is the topological derivative at point given in Equation 4. DTD method is used from a cost function for discrete approach (20). It was given by the equation 5:

$$(4) \quad \Psi_\delta(\Omega_\delta) = \Psi(\Omega) + f(\epsilon) D_T(x) 0f(\epsilon)$$

$$(5) \quad \Psi(u_i^s) = \sum_s \sum_{p \in n^s} k^{s,p} \Delta u_i^{s,p} \Delta u_i^{s,p}$$

Where $k^{s,p}$ is the diffusion of pixel s with neighbors p and $n^s = \{w, e, n, s\}$ indicating the neighbors of the pixel s and u_i^s is the intensity of the image pixel. Also, $\Delta u_i^{s,p}$ is defined by the Equation 6:

$$(6) \quad \Delta u_i^{s,p} = u_i^p - u_i^s$$

And u_i^s is clearly calculated using the Equation 7:

$$(7) \quad U_i^s(k^s) = u_{i-1}^s + \Delta t \sum_{p \in n^s} k^{s,p}$$

Where $I \geq 1$ indicates the iteration number, $k = \{k^{s,w}, k^{s,e}, k^{s,n}, k^{s,s}\}$ indicates the set of diffusion factor associated with the pixel s and Δt is the artificial time step size.

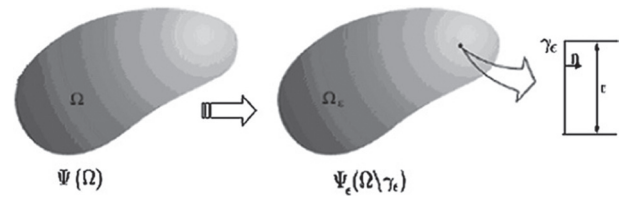


Figure 1. Representation of Topological Derivative Diagram

3.3. Statistical Analysis

All continues data are expressed as mean \pm standard deviation (SD). Normal distribution and homogeneity of variance of data were checked by Kolmogorov-Smirnov test (K-S) and Levene's test, respectively. The statistical significance in mean values of MSE, PSNR, NAE, NCC, SSIM, SI, SC, IQI, MD, AD and ENL variables of the Canny edge detection with all filters were assessed by ANOVA test. LSD (Least Significant Difference) was used as post hoc test. P value < 0.05 was considered statistically significant. All statistical analyses were performed using SPSS software package (SPSS V.18, Inc. Chicago, IL). The maximum sample size for the analysis of variance (ANOVA) was estimated from Equation 8:

$$(8) \quad N = \frac{\lambda}{\Delta}$$

N and λ were sample size and non-centrality parameter, respectively and estimated with a confidence level of 95%

and power test of 80%. The value of Δ was calculated from Equation 9:

$$(9) \quad \Delta = \frac{1}{\sigma^2} \sum_{i=1}^k (\mu_i - \mu_m)^2, \mu_m = \frac{1}{k} \sum_{j=1}^k \mu_j$$

k , σ , μ_i , and μ_m were number of groups, standard deviation, mean of each group and overall mean (33).

4. Results

Ultrasonic examination was performed for the left common carotid and brachial arteries of forty-two men (aged 44 ± 6 years) with no history of cardiovascular and/or cerebrovascular disease, hypertension, diabetes mellitus and tobacco abuse. Body mass index (BMI) of participants was 23 ± 3 ; systolic pressure as 122 ± 14 mmHg; diastolic pressure as 83 ± 5 mmHg and Heart rate (HR) of 71 ± 6 bpm (beat per minute). Figure 2 shows original and filtered common carotid and brachial arteries in a study subject. The results of de-noising filters with the Canny edge detection are summarized in Table 2 for IMT of the left common carotid and left brachial arteries in 90 frames (almost three cardiac cycles). According to values of MSE, PSNR, NAE, NCC, SSIM, SI, SC, IQI, MD, AD and ENL, there was a significant difference between CTD, DTD and SRAD filters-Canny edge detection status in the common carotid artery (all P values < 0.001). According to values of MSE, PSNR, NAE, NCC, SSIM, SI, SC, IQI, MD, AD and ENL, there

was a significant difference between CTD, DTD and SRAD filters-Canny edge detection status in brachial artery (all P values < 0.001). DTD and CTD filters with the Canny edge detection were better than SRAD filter with the Canny detection for speckle suppression and details preservation in the common carotid and brachial arteries ultrasound images (Lower MSE, SI, MD, AD, NAE higher PSNR, ENL and near to 1 for NCC, SC, IQ, SSIM; all proved that their performance are high in de-noising ultrasound images).

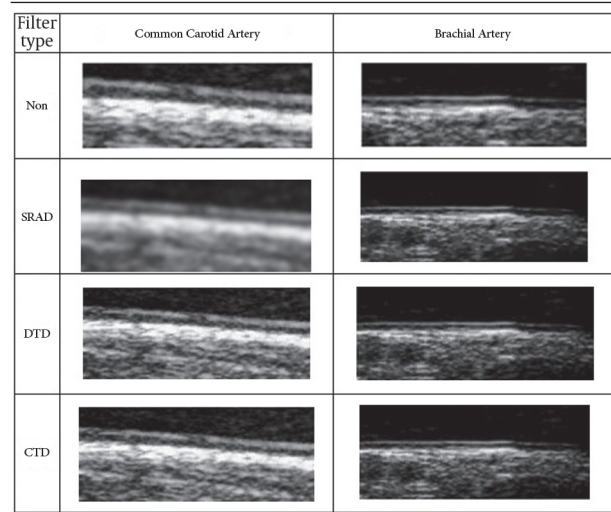


Figure 2. Left Common Carotid and Brachial Arteries Ultrasound Image for One Sample

Table 2. Mean and Standard Deviation of Image Quality Metrics for Three Filters With the Canny Edge Detection in Left Common Carotid and Brachial Arteries of 42 Study Subjects. ^{a,b,c}

| Filters | SRAD Carotid | DTD Carotid | CTD Carotid | SRAD Brachial | DTD Brachial | CTD Brachial |
|---------|--------------------------|--------------------------|--------------------------|--------------------------|--------------------------|--------------------------|
| MSE | 0.00324108 ± 0.00015115 | 0.00008730 ± 0.00001541 | 0.00000473 ± 0.00000068 | 0.00383169 ± 0.00059373 | 0.00003584 ± 0.00000089 | 0.00000039 ± 0.00000011 |
| PSNR | 73.01653278 ± 0.20225305 | 88.86324610 ± 0.81565367 | 95.42742459 ± 0.63852141 | 88.27062507 ± 0.62662068 | 92.57914974 ± 0.11065172 | 96.38840262 ± 1.24717083 |
| NAE | 0.02367264 ± 0.00065456 | 0.02758987 ± 0.00103658 | 0.00314536 ± 0.00044993 | 0.08993134 ± 0.00047839 | 0.03650177 ± 0.00045128 | 0.00052831 ± 0.00009334 |
| NCC | 0.93597502 ± 0.00190416 | 0.95926880 ± 0.01742364 | 0.98488556 ± 0.00002543 | 0.94851670 ± 0.00016193 | 0.95996759 ± 0.00001070 | 0.986584858 ± 0.01323544 |
| SSIM | 0.91999900 ± 0.00000013 | 0.94997444 ± 0.00000121 | 0.97438041 ± 0.00058733 | 0.92996422 ± 0.00000130 | 0.94999964 ± 0.00000012 | 0.97960682 ± 0.00060962 |
| SI | 0.00000497 ± 0.00000089 | 0.00000556 ± 0.00000096 | 0.00000544 ± 0.00000098 | 0.00000519 ± 0.00000091 | 0.00000700 ± 0.00000122 | 0.00000703 ± 0.00000122 |
| SC | 1.07920751 ± 0.00211329 | 1.00013505 ± 0.00003092 | 0.99934641 ± 0.00018419 | 0.67309709 ± 0.00229816 | 1.00088738 ± 0.00030854 | 1.00004156 ± 0.00001575 |
| IQI | 0.46115492 ± 0.00881941 | 0.92080477 ± 0.00087706 | 0.95046500 ± 0.00105049 | 0.21272323 ± 0.00321600 | 0.92794113 ± 0.00059459 | 0.96941824 ± 0.00020984 |
| MD | 0.62094131 ± 0.02801523 | 0.53425688 ± 0.04575904 | 0.16480626 ± 0.06260978 | 0.48859484 ± 0.05026766 | 0.39531867 ± 0.03183652 | 0.09944374 ± 0.03892293 |
| AD | 0.03302151 ± 0.00112835 | 0.00371374 ± 0.00016375 | 0.00043881 ± 0.00006806 | 0.05708596 ± 0.00015745 | 0.00231214 ± 0.00002969 | 0.00003372 ± 0.00000587 |
| ENL | 0.48527880 ± 0.00539073 | 0.54529820 ± 0.00607544 | 0.59050902 ± 0.00813031 | 0.23697928 ± 0.00178620 | 0.30018565 ± 0.00046646 | 0.55891358 ± 0.00293672 |

^a Abbreviations: MSE, mean squared error; PSNR, peak signal to noise ratio; NAE, normalized absolute error; NCC, normalized cross-correlation; SSIM, structure similarity image measures; SI, speckle index; SC, structural content; IQI, image quality index; MD, maximum difference; AD, average difference; ENL, equivalent number of looks.

^b Data are presented as Mean ± SD.

^c All P Values for ANOVA and Post Hoc Multiple Comparisons LSD Test Were < 0.001.

5. Discussion

Nowadays, one of the main methods for prediction of cardiovascular diseases is measuring IMT of the common carotid artery. Therefore, precise measurement of IMT is useful for assessing the risk of cardiovascular diseases or its progress (34). Moreover, Weidinger et al. (4) showed that assessment of brachial artery may have some potential advantages. First, changes of function and morphology can be detected in the same artery. Second, the pattern of wall thickening in the brachial artery is rather defused than carotid artery, which may be a more sensitive indicator of long-term systemic exposure to risk factors. Besides, study of the blood flow in arteries is a rich field surrounding unsteady flows, changing geometries and secondary structures. Diseased arteries can create high levels of turbulence, head loss and a choked-flow condition in which arteries can collapse. The pulsatile nature of the flow creates a dynamic environment that raises many interesting and fundamental unsteady fluid and arterial wall mechanics questions. Answers to these questions can be used to predict and change blood flow to alter the course of disease. Each fluid and wall mechanics aspect plays a role in the generation, detection and treatment of arterial disease. Besides, quantities of stress and mass transfer at the blood-wall interface are essential hemodynamic factors influencing biological responses (35). Saccular intracranial aneurysms usually occur at arterial curves and bifurcations in the circle of Willis, with strong implication of a critical role for hemodynamics in such vascular geometry (36). Wall shear stress and strain distributions and extreme values are broadly accepted to be responsible for aneurysm initiation, growth and rupture (37). Moreover, artery stenosis may induce disturbance and flow separation, and consequently create significant flow resistance, large pressure drop and complex flow pattern (38). Castro et al. showed that for higher stenosis grades, the recirculation pattern results in more velocity and wall shear stress values over a big area. For distal aneurysms ipsilateral to the high degree stenosis, the vortex may reach the aneurysm basing on the stenosis grade and the distance between the aneurysm and the stenosis. Under this situation, the part of the neck closer to the aneurysm witnesses high velocities upstream, resulting in the higher wall shear stress values. For the use of computational fluid dynamics in the study involving aneurysm and stenosis has gained significance, focusing on different shape and size of aneurysms and stenosis severity with idealized geometries (35, 39). Due to the above-mentioned matters, fluid and arterial wall structure and mechanics would continue to play a major role in the future diagnosis, understanding and treatment of cardiovascular diseases. Ultrasound is a broadly used and safe medical imaging technique due to its noninvasive nature, low cost and capability of forming real time imaging (40). However, the efficacy of ultrasound imaging is reduced by presence of signal dependent noise known as speck-

le. Speckles tend to mask the presence of low-contrast lesion and reduce the ability of observers to resolve the real information. Moreover, presence of speckles in common carotid artery ultrasound images hinders enhancement in them. They also complicate image processing like image segmentation and edge detection. Therefore, it is very important to suppress speckle noise and the image with losing worth image features is enhanced before making any image analysis (5). Speckle is not a kind of additive noise. It is a form of multiplicative noise (8). The traditional speckle removal filters, like the Lee filter and Frost filter have greater restrictions in edge preserving and characteristics preserving (9). Noise reduction filter such as conventional anisotropic diffusion is not proper to speckle suppression (8). It is proper for additive noise. According to these problems, SRAD, DTD and CTD have attracted researchers' attention. These filters not only preserve edges, but also reduce noise (6, 24, 41). Edge detection has been used as a tool for evaluating the performance of noise reduction filters. Maini and Aggraval et al. proposed that the Canny edge detection algorithm is a proper method, which reduces false and misses real edges. It also reduces multiple responses to real edge (42, 43). This study showed that DTD and CTD filters with the Canny edge detection are better than SRAD filter with the Canny detections for speckle noise reduction and details in the common carotid and brachial arteries ultrasound images. The present study is in agreement with others (11, 20). Using the automatic method for measuring the IMT in B-mode ultrasound images, a few researches showed that changes in IMT happen during cardiac cycle (44-46). Selzer et al. (47) showed that common carotid IMT was lower at peak-systolic than end-diastolic by an average of 5.3% in 24 samples. Another study showed that averaged change of IMT in the common carotid was 0.041 mm (48). Therefore, in this study we tried to provide a condition that noise reduction followed at approximately three cardiac cycles. Moreover, noise reduction was used on ultrasound images of IMT in both arteries (carotid and brachial arteries). Probably, our study contained more comprehensive information than other studies that noise reduction was performed only on one frame or one artery. One limitation of this study was that despite we used four orders PDE in SRAD algorithm, consumed time in de-noising of this filter was a little more than the ultrasound images. Another limitation was that the translation movement of the common carotid and brachial arteries which came from the probe movement during scanning and suppression of artery of artery pulsating movement were more complicated. However, we concluded that these movements were less. We concluded that DTD and CTD filters with the Canny edge detection were better than SRAD filter with the Canny detection for speckle suppression and details preservation in the common carotid and brachial arteries ultrasound images. Our finding may help physicians to measure carotid and brachial IMT better than non-denoising ultrasound images.

Acknowledgements

We wish to thank all the staff nurses in the Beheshti hospital, Kashan University of Medical Sciences, for their kind help and kind cooperation during the research.

Authors' Contributions

Study concept and design: Hasan Voshtani and Mehvar Rafati. Analysis and interpretation of data: Masoud Arabfard and Hassan Moladoust. Drafting of the manuscript: Hasan Voshtani, Mehrdad Rafati Rahimzadeh. Critical revision of the manuscript for important intellectual content: Mehvar Rafati, Masoud Arabfard and Hassan Moladoust. Statistical analysis: Mehvar Rafati and Mehrdad Rafati Rahimzadeh.

References

- de Korte CL, Hansen HHG, van der Steen AFW. Vascular ultrasound for atherosclerosis imaging. *Interface Focus*. 2011;**4**(4):565-75.
- Gayathri R, Chandni R, Udayabhaskaran V. Carotid artery intima media thickness in relation with atherosclerotic risk factors in patients with type 2 diabetes mellitus. *J Assoc Physicians India*. 2012;**60**:20-4.
- Carallo C, Irace C, Pujia A, De Franceschi MS, Crescenzo A, Motti C, et al. Evaluation of common carotid hemodynamic forces. Relations with wall thickening. *Hypertension*. 1999;**34**(2):217-21.
- Weidinger F, Frick M, Alber HF, Ulmer H, Schwarzscher SP, Pachinger O. Association of wall thickness of the brachial artery measured with high-resolution ultrasound with risk factors and coronary artery disease. *Am J Cardiol*. 2002;**89**(9):1025-9.
- Wan MH, Supriyanto E. Comparative evaluation of ultrasound kidney image enhancement techniques. *Int J Comput Appl*. 2011;**21**(7):15-9.
- Benes R, Riha K. Medical image denoising By improved Kuan filter. *Adv Electr Electron Eng*. 2012;**10**(1):43-9.
- Kaur J, Kaur J, Kaur M. Survey of de-speckling techniques for medical ultrasound images. *Int J Comp Tech Appl*. 2011;**2**:1003-7.
- Sun Q, Hossack JA, Tang J, Acton ST. Speckle reducing anisotropic diffusion for 3D ultrasound images. *Comput Med Imaging Graph*. 2004;**28**(8):461-70.
- Yu Y, Acton ST. Speckle reducing anisotropic diffusion. *IEEE Trans Image Process*. 2002;**11**(11):1260-70.
- Zol SH. A comparative study of segmentation methods for brain tumor detection. *Indian Stream Research Journal*. 2008;**1**:1-6.
- Krishnaveni M, Radha V. A Topological derivative based image segmentation for sign language recognition system using isotropic filter. *Int J Comput Inf Secur*. 2010;**6**:41-5.
- Patel BC, Sinha GR, Thakur K. Early detection of breast cancer using a modified topological derivative based method. *Int J Pure Appl Sci Technol*. 2011;**7**(1):75-80.
- Rabelo LM. Atherosclerotic risk factors in adolescence. *J Pediatr (Rio J)*. 2001;**77**(Suppl 2):S153-64.
- Mokhtari-Dizaji M, Montazeri M, Saberi H. Differentiation of mild and severe stenosis with motion estimation in ultrasound images. *Ultrasound Med Biol*. 2006;**32**(10):1493-8.
- Laurent S, Cockcroft J, Van Bortel L, Boutouyrie P, Giannattasio C, Hayoz D, et al. Expert consensus document on arterial stiffness: methodological issues and clinical applications. *Eur Heart J*. 2006;**27**(21):2588-605.
- Kitaoka M, Matsuo H, Taniguchi N, Ozaki T, Kaneda S, Ennda E. Standard method for ultrasound evaluation of carotid artery. *J Med Ultrason*. 2006.
- Touboul PJ, Hennerici MG, Meairs S, Adams H, Amarenco P, Bornstein N, et al. Mannheim carotid intima-media thickness consensus (2004-2006). *Cerebrovasc Dis*. 2007;**23**:75-80.
- Naim C, Douziche M, Therasse E, Robillard P, Giroux MF, Arsenault F, et al. Vulnerable atherosclerotic carotid plaque evaluation by ultrasound, computed tomography angiography, and magnetic resonance imaging: an overview. *Can Assoc Radiol J*. 2014;**65**(3):275-86.

- Joseph A, Babu JS, Soman KP. Analysis of reconstructed images using compressive sensing. *Int J Sci Engin Res*. 2012;**3**:1-6.
- Damodaran N, Ramamurthy S, Velusamy S, Manickam GK. Speckle noise reduction in ultrasound biomedical B-scan images using discrete topological derivative. *Ultrasound Med Biol*. 2012;**38**(2):276-86.
- Sivakumar R, Gayathri MK, Nedumaran D. Speckle filtering of ultrasound B-scan images-A comparative study of single scale spatial adaptive filters, multi-scale filter and diffusion filters. *Int J Eng Technol*. 2010;**2**:514-23.
- Raj VNP, Venkateswarlu T. Ultrasound medical image denoising using hybrid bilateral filtering. *Int J Comput Appl*. 2012;**56**(14):44-51.
- Poobal S, Ravindran G. The performance of fractal image compression on different imaging modalities using objective quality measures. *Int J Eng Scie Technol*. 2011;**3**:525-30.
- Sumantyo JTS, Amini J. A model for removal noise in SAR images (Alos Palsar). *Can J Remote Sensing*. 2008;**34**(6):503-15.
- Zahedi E, Jaafar R, Ali MA, Mohamed AL, Maskon O. Finger photoplethysmogram pulse amplitude changes induced by flow-mediated dilation. *Physiol Meas*. 2008;**29**(5):625-37.
- Shruthi G, Usha BS, Sandya S. A novel approach for speckle reduction and enhancement of ultrasound images. *Int J Comput Appl*. 2012;**45**:14-20.
- Sarode MV, Deshmukh PR. Reduction of speckle noise and image enhancement of images using filtering technique. *Int J Adv Technol*. 2011;**2**(1):30-8.
- Abd-Elmoniem KZ, Youssef AB, Kadah YM. Real-time speckle reduction and coherence enhancement in ultrasound imaging via nonlinear anisotropic diffusion. *IEEE Trans Biomed Eng*. 2002;**49**(9):997-1014.
- Benes R, Riha K. Noise reduction in medical ultrasound images. *Electron Revenue*. 2011;**2**:1-8.
- Geethalakshmi SN, Suguna J. Hybrid models for denoising ultrasonic images. *J Glob Res Comput Sci*. 2010;**1**:38-45.
- Larrabide I, Novotny AA, Feijóo RA, Taroco E, editors. A medical image enhancement algorithm based on topological derivative and anisotropic diffusion.; Proceedings of the XXVI Iberian Latin-American Congress on Computational Methods in Engineering-CILAMCE.; 2005; Citeseer; pp. 1-14.
- Larrabide I, Feijoo RA, Novotny AA, Taroco E. Topological derivative: A tool for image processing. *Comput Struct*. 2008;**86**.
- Chow SC, Shao J, Wang H. *Sample size calculations in clinical research*. New York: Chapman & Hall / CRC Biostatistics Series; 2003.
- Polak JF, Pencina MJ, Meisner A, Pencina KM, Brown LS, Wolf PA, et al. Associations of carotid artery intima-media thickness (IMT) with risk factors and prevalent cardiovascular disease: comparison of mean common carotid artery IMT with maximum internal carotid artery IMT. *J Ultrasound Med*. 2010;**29**(12):1759-68.
- Soudah E, Ng EY, Loong TH, Bordone M, Pua U, Narayanan S. CFD modelling of abdominal aortic aneurysm on hemodynamic loads using a realistic geometry with CT. *Comput Math Methods Med*. 2013;**2013**:472564.
- Meng H, Wang Z, Kim M, Ecker RD, Hopkins LN. Saccular aneurysms on straight and curved vessels are subject to different hemodynamics: implications of intravascular stenting. *AJNR Am J Neuroradiol*. 2006;**27**(9):1861-5.
- Castro MA, Peloc NL, Putman CM, Cebra JR. Changes in cerebral aneurysm hemodynamics after virtual endarterectomy. *Mecanica Computacional*. 2012:3797-809.
- Siauw WL, Ng EY, Mazumdar J. Unsteady stenosis flow prediction: a comparative study of non-Newtonian models with operator splitting scheme. *Med Eng Phys*. 2000;**22**(4):265-77.
- Li MX, Beech-Brandt JJ, John LR, Hoskins PR, Easson WJ. Numerical analysis of pulsatile blood flow and vessel wall mechanics in different degrees of stenoses. *J Biomech*. 2007;**40**(16):3715-24.
- Narayanan SK, Wahidabanu RSD. A view on de-speckling in ultrasound imaging. *Int J Signal Process Image Process Pattern Recognit*. 2009.

41. Chai HY, Wee LK, Supriyanto E. Ultrasound images edge detection using anisotropic diffusion in canny edge detector framework. *Wseas Trans Biol Biomed*. 2011;**8**:51-60.
42. Maini JR, Aggarwal H. Study and comparison of various image edge detection techniques. *Int J Image Process*. 2009;**3**.
43. Rafati M, Arabfard M, Rafati-Rahimzadeh M. Comparison of different edge detections and noise reduction on ultrasound images of carotid and brachial arteries using a speckle reducing anisotropic diffusion filter. *Iran Red Crescent Med J*. 2014;**16**(9).
44. Wendelhag I, Liang Q, Gustavsson T, Wikstrand J. A new automated computerized analyzing system simplifies readings and reduces the variability in ultrasound measurement of intima-media thickness. *Stroke*. 1997;**28**(11):2195-200.
45. Kanai H, Koiwa Y. Real-time velocimetry for evaluation of change in thickness of arterial wall. *Ultrasonics*. 2000;**38**(1-8):381-6.
46. Boutouyrie P, Germain DP, Tropeano AI, Laloux B, Carenzi F, Zidi M, et al. Compressibility of the carotid artery in patients with pseudoxanthoma elasticum. *Hypertension*. 2001;**38**(5):1181-4.
47. Selzer RH, Mack WJ, Lee PL, Kwong-Fu H, Hodis HN. Improved common carotid elasticity and intima-media thickness measurements from computer analysis of sequential ultrasound frames. *Atherosclerosis*. 2001;**154**(1):185-93.
48. Polak JF, Johnson C, Harrington A, Wong Q, O'Leary DH, Burke G, et al. Changes in carotid intima-media thickness during the cardiac cycle: the multi-ethnic study of atherosclerosis. *J Am Heart Assoc*. 2012;**1**(4):e001420.